Met. Mater. Int., Vol. 23, No. 3 (2017), pp. 465~472
doi: 10.1007/s12540-017-6573-4

Directionality of Residual Stress Evaluated by Instrumented Indentation Testing Using Wedge Indenter

Hee-Jun Ahn[1], Jong-hyoung Kim[1], Huiwen Xu[1], Junsang Lee[1], Ju-Young Kim[2], Young-Cheon Kim[3,*], and Dongil Kwon[1]

[1]Department of Materials Science and Engineering, Seoul National University, Seoul 08826, Republic of Korea
[2]School of Materials Science and Engineering, UNIST (Ulsan National Institute of Science and Technology), Ulsan 44919, Republic of Korea
[3]Mechanical Safety Technology Center, System Convergence Technology Division, KTL (Korea Testing Laboratory), Jinju 52852, Republic of Korea

(received date: 16 August 2016 / accepted date: 7 November 2016)

In instrumented indentation testing (IIT), residual stress can be evaluated by shift in indentation load-depth curves for stress-free and stressed states. Although the average surface residual stress is able to be evaluated with Vickers indenter, in order to know stress directionality, another indentation tests with two-fold symmetric indenter, for example, Knoop indenter, are needed. As some necessities for evaluating nonequibiaxial residual stress within small indent area, we suggest a novel way to evaluate directionality of residual stress, p, using wedge indenter characterized by two parameters, edge length and inclined angle. We develop wedge-indentation-mechanics model based on predetermined conversion factors which are determined by IITs for various uniaxial stressed states combining with finite element analysis simulations. By utilizing the developed model, directionality of residual stress is evaluated through two serial wedge IITs with respect to principal directions. We find good agreements between applied residual stress and residual stress evaluated by the developed model for biaxial tensile stress states.

Keywords: indentation, residual stress, metals, deformation, wedge indenter

1. INTRODUCTION

Residual stress can be defined as the self-equilibrating internal stress existing in a free body when no external forces are applied. Residual stresses can arise in materials during processing, for example, heat treatment or machining [1] and can change material properties such as fatigue strength and fracture toughness [2]. Hence quantifying residual stress is significant in assessing the reliability and integrity of industrial structure and facilities.

Many methods for measuring residual stress quantitatively have been developed over the past few decades. Hole-drilling, sectioning, and contour methods are destructive methods used in evaluating residual stress, X-ray diffraction, neutron diffraction, and curvature methods are non-destructive tests. All these conventional methods have difficulty in evaluating residual stress in the field or in local mapping. The instrumented indentation test has been investigated in order to overcome these difficulties.

Tsui *et al.* [3-5] looked for a relationship between applied stress state and mechanical properties like conventional hardness, indentation hardness, elastic modulus and stiffness with instrumented indentation testing, and they found that conventional hardness, elastic modulus and stiffness were invariant. Bolshakov *et al.* [6] did similar work with FEA simulation for observing the exact indentation contact area. Suresh and Giannakopoulos [7] first developed a theoretical model for estimating surface average residual stress by measuring the apparent contact area during instrumented sharp indentation. Swadener *et al.* [8] suggested the residual stress measurement method with spherical indentation test to improve residual stress sensitivity. Giannakopoulos [9] analyzed analytically and experimentally the effect of the surface initial stresses in the load-depth response in instrumented sharp indentation. And Lee and Kwon [10] and Jang [11] used tensor analysis of the stress beneath the indenter for the same purpose and linked the zz-direction deviatoric stress component to indentation load. Since a stress-induced normal load difference L_0–L_S affects only z-direction deviatoric stress, the relation can be derived as

$$\sigma_{res}^{x} = \frac{3}{1+p}\frac{(L_0-L_S)}{A_S} \tag{1}$$

$$\sigma_{res}^{y} = p\,\sigma_{res}^{x} = \frac{3p}{1+p}\frac{(L_0-L_S)}{A_S} \tag{2}$$

*Corresponding author: im01000@ktl.re.kr

where L_0, and L_S are the load value of the stress-free and stressed stat at a given indenting depth respectively, p is the stress directionality (i.e., the surface residual stress ratio in each principal direction, σ_y/σ_x), and the A_S is the contact area in the stressed state.

Lee *et al.* [12,13] researched evaluating residual stress directionality in specimens in nonequibiaxial residual stress states by observing the contact morphology. Han *et al.* [14] and Choi *et al.* [15], working on evaluating stress directionality by an instrumented Knoop indentation test, found a relationship between uniaxial residual stress and load difference and called it conversion factor. By twice performing instrumented Knoop indentation tests on principal direction, they set up a model for biaxial residual stress directionality with conversion factor ratio.

Kim *et al.* [16] performed research on estimation of principal direction and stress directionality with 4-times instrumented Knoop indentation test and discussed the physical meaning of the conversion factor ratio with the size of plastic zone beneath indenter. Kim *et al.* [17] recently worked to establish a method to evaluate of biaxial residual stress magnitude, directionality, and principal direction with only instrumented Knoop indentation testing.

However, although we often want to know the stress directionality in a small indent area, for example a curved structure or in-filed experiments, the Knoop indenter has difficulty in using for small indent sizes because it has two obtuse angles. If the instrumented Knoop indentation test is performed on lower indentation depths, as the load difference decreases rapidly, small experimental issues such as in specimen surface preparation or indentation normality can be caused.

In order to overcome this difficulty, we suggest here performing indentation testing with a novel indenter shape, a wedge indenter. There are two reasons for evaluating residual stress directionality with wedge indenter. The first is a decrease in the indent size. Unlike the Knoop indenter, the wedge shape makes it possible to select the edge length independent of indenting depth. The second reason is increased sensitivity to residual stresses; i.e., in this case the increased load difference between stress-free and stressed-state specimens, to residual stress in each direction. When the specifications are controlled, it is possible to maximize the residual stress sensitivity in one direction in biaxial residual stress. Here we propose to residual stress evaluation with a wedge indenter and verify our model by applying stress to cruciform samples using a stress-inducing jig and by FEA simulation.

2. THEORETICAL MODELING - WEDGE INDENTATION TECHNIQUE

In instrumented Knoop indentation testing, Han *et al.* [14] and Choi *et al.* [15] introduced conversion factors that are variables relating the residual stress to the indentation load difference as $\alpha_{//}$ and $\alpha_{\perp}$. They obtained stress directionality with the constant conversion factor ratio, of 0.34, regardless of residual stress state and indentation depth.

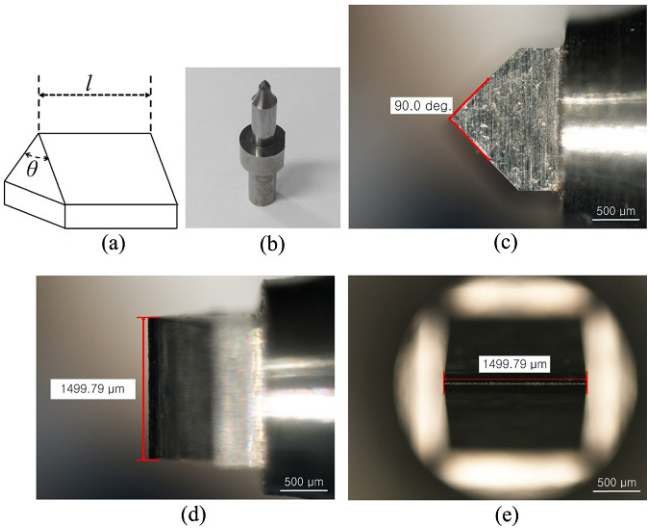

Fig. 1. (a) Schematic diagram of wedge indenter edge, (b) Wedge indenter produced by H.M.TEC. (c) Indenter angle (× 50), (d) Indenter length (side view) (× 50), and (e) Indenter length (top view) (× 50).

Following a similar procedure, the residual stress directionality is obtained by wedge indenter. The wedge indenter has two dimensions: an edge length (l) and an included angle (θ), as in Fig. 1(a), so that by selecting a suitable shape, residual stress sensitivity can be increased. When wedge indentations are made on a specimen in nonequibiaxial stress, the indentation load-depth curves change depending on indenter direction. In the case ($\sigma_{res}^{x} > \sigma_{res}^{y}$), when the edge length direction coincides with σ_{res}^{x}, the load value at a given indenting depth h, L_x, attains its maximum. On other hand, when the edge length direction is perpendicular to σ_{res}^{x}, the load value at a given indenting depth h, L_y, is a minimum at the given indenting depth. The load differences ΔL_x and ΔL_y between a stressed

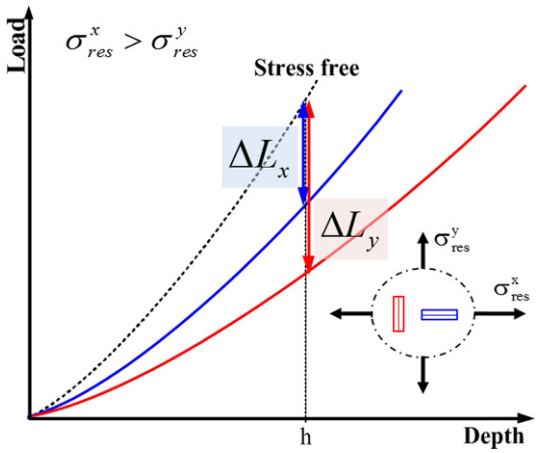

Fig. 2. Schematic indentation load-depth curve from two wedge indentations in the biaxial stress state.

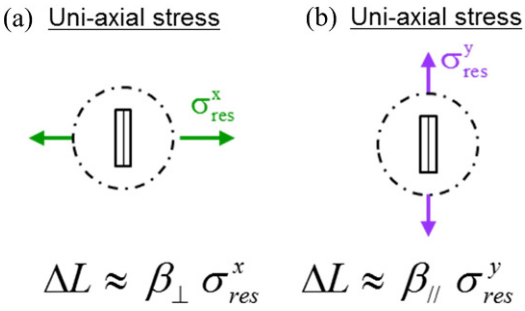

Fig. 3. Definition of conversion factor (a) conversion factor, $\beta_{\perp}$, is defined as a proportional coefficient when uniaxial stress is perpendicular to edge length direction and (b) conversion factor, $\beta_{//}$, is defined as a proportional coefficient when uniaxial stress is parallel to edge length direction.

and stress-free specimen are calculated by considering the effect of each principal stress on the indenting load (Fig. 2):

$$\Delta L_x = \beta_{//}\sigma^x_{res} + \beta_{\perp}\sigma^y_{res} \tag{3}$$

$$\Delta L_y = \beta_{\perp}\sigma^x_{res} + \beta_{//}\sigma^y_{res} \tag{4}$$

where $\beta_{//}$ and $\beta_{\perp}$ are conversion factors linking the residual stress to the indentation load difference and their subscripts mean directions between the principal stress and the edge length direction of wedge indenter; the concept is similar to conversion factors, $\alpha_{//}$, $\alpha_{\perp}$ in instrumented Knoop indentation (Fig. 3).

In order to obtain information on stress directionality, the ratio of load differences can be addressed:

$$\frac{\Delta L_x}{\Delta L_y} = \frac{\beta_{//}\sigma^x_{res} + \beta_{\perp}\sigma^y_{res}}{\beta_{\perp}\sigma^x_{res} + \beta_{//}\sigma^y_{res}}, \tag{5}$$

$$\frac{\Delta L_x}{\Delta L_y} = \frac{\dfrac{\beta_{//}}{\beta_{\perp}} + \dfrac{\sigma^y_{res}}{\sigma^x_{res}}}{1 + \dfrac{\beta_{//}}{\beta_{\perp}}\dfrac{\sigma^y_{res}}{\sigma^x_{res}}}, \tag{6}$$

$$p = \frac{\sigma^y_{res}}{\sigma^x_{res}} = \frac{\dfrac{\Delta L_x}{\Delta L_y} - \dfrac{\beta_{//}}{\beta_{\perp}}}{1 - \dfrac{\beta_{//}}{\beta_{\perp}}\dfrac{\Delta L_x}{\Delta L_y}} \tag{7}$$

The stress directionality, p, can be evaluated from conversion factor ratio $\beta_{//}/\beta_{\perp}$. Each conversion factor ($\beta_{//}$, $\beta_{\perp}$) was obtain from the linear slopes between load differences (ΔL_x, ΔL_y) and applied uniaxial stresses.

3. EXPERIMENTAL PROCEDURE

Instrumented indentation tests were performed using the AIS 3000 system (Frontics, Inc., Korea) with force resolution 49 mN and displacement resolution 0.1 μm), and the

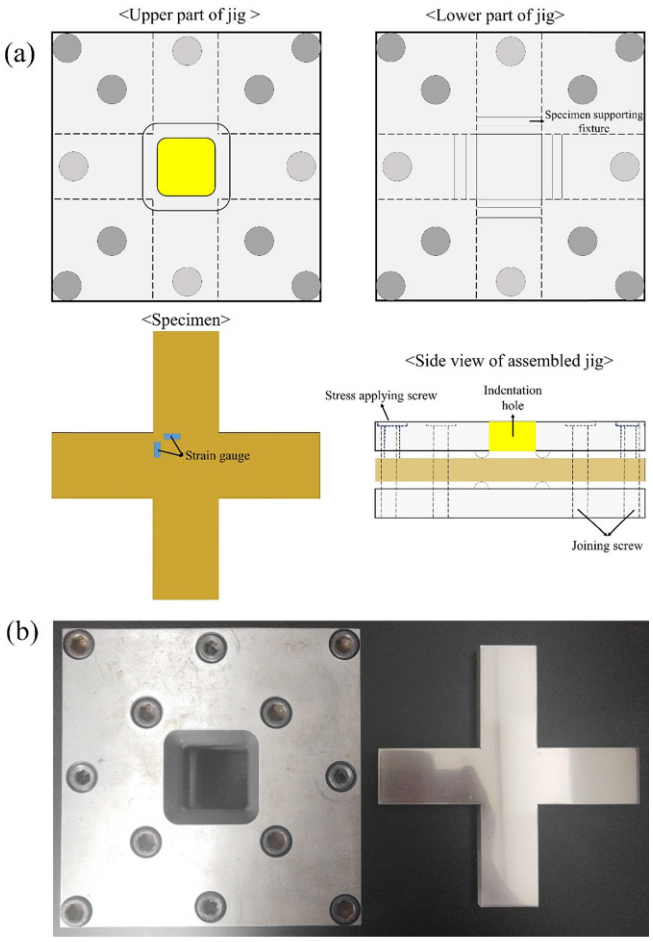

Fig. 4. (a) Schematic diagram of stress-generating jig and specimen shape and (b) photo of stress generating jig and specimen.

tungsten carbide wedge indenter was made by H.M.TEC (Korea) (Fig. 1(b)) and length and angle were verified with optical microscopy (Fig.1(c, d)). In order to take advantage of the indent size, the edge length of the custom wedge indenter was targeted at one half of the long diagonal of the Knoop indenter with an indentation depth of 100 μm. As long diagonal of Knoop indenter was about 3.05 mm at 100 μm indentation depth, the edge length of wedge indenter was determined as 1.5 mm independent of indentation depth. The indenter included angle was chosen as 90 degrees in order to match the half-indent impression of the Knoop indenter. Indentation tests are performed with this suggested wedge indenter and a commercial Knoop indenter, and the indent area of indentation is observed with optical microscopy. The machine compliance, including indenter compliance, was 0.095 μm/kgf. To verify the theoretical model, a stress-generating jig with two independent orthogonal loading axes was designed to strain rectangular beam and cruciform specimens (Fig. 5).

The applied biaxial surface strains were converted to biaxial stresses of the two orthogonal axes using the Young's modulus and Poisson's ratio of the specimens. To keep the applied

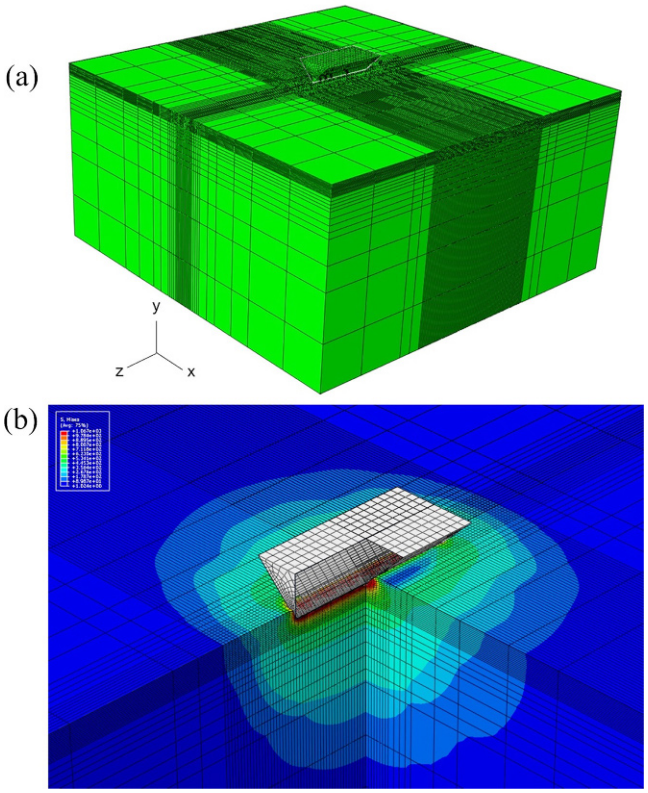

Fig. 5. Finite Element Analysis modeling of wedge indentation. (a) Meshed wedge indenter and specimen and (b) deformed shape of specimen in wedge indentation.

stress below the elastic limit, we maintained the specimen yield strength which is concerned the Tresca yield criterion. In order to obtain the conversion factor ratio, indentation tests were performed in various uniaxial tensile stress states to determine the linear relationship among ΔL_x, ΔL_y and residual stress. The experimental process was performed experimentally on three samples: SCM4, S45C and SKD11 (Table 1). As the residual stress is not a material property but a stress state, it can be deduced that the residual stresses are independent of the materials. For convenient and rapid material supply, the experimental materials were carbon steel.

For the verification of suggested model, one equibiaxial stress and three nonequibiaxial stresses were applied and indentation tests were performed twice on principal directions (σ_I, σ_{II}) (Table 2).

In addition, numerical simulations were performed using the commercial finite element code ABAQUS 6.12. The specimen was generated in various uniaxial applied stress states, and wedge indentation was conducted twice perpendicular and parallel to the applied uniaxial stress direction. The specimens were S45C and STS303. The simulation of wedge indentation was made up 104,832 elements of C3D8R mesh-type specimen, 1901 elements of R3D4 and 20 elements of R3D3 mesh-type indenter (Fig. 6(a)). The elastic modulus and yield strength of STS 303 were 206 GPa and 328 MPa, and those of S45C were 202 GPa, and 320 MPa. The material models of specimens were both isotropic plastic hardening and the friction coefficient between specimen and indenter was 0.2. The Knoop indentation simulations comparing the load difference sensitivity in residual stress with wedge indentation were performed with 21,071 mesh elements.

4. RESULTS AND DISCUSSION

As in Fig. 7, the indent lengths of edge length and included angle direction at 100 μm indentation depth are 1500.26 μm and 211.68 μm, respectively, and the length of long diagonal and short diagonal of Knoop indenter at same indentation

Table 1. Experimental and simulation conditions for determination of conversion factors: various materials and applied tensile stress states

Number	Materials	Elastic modulus (GPa)	Yield strength (MPa)	Applied uniaxial tensile stress (MPa)
Experimental #1	S45C	202	320	75
Experimental #2	S45C	202	320	150
Experimental #3	SKD11	209	700	203
Experimental #4	SCM4	200	362	270
Simulation #1	S45C	202	320	150
Simulation #2	STS303	206	328	180
Simulation #3	STS303	206	328	200
Simulation #4	STS303	206	328	250

Table 2. Experimental conditions for verification of modeling: various materials and applied tensile stress states

Number	Materials	Applied tensile stress of x-axis (MPa)	Applied tensile stress of y-axis (MPa)	Stress directionality (p)
Experimental #1	SCM4	270	0	0
Experimental #2	SCM4	143	46	0.32
Experimental #3	S45C	127	85	0.67
Experimental #4	S45C	151	150	0.50
Experimental #5	S45C	149	75	0.5

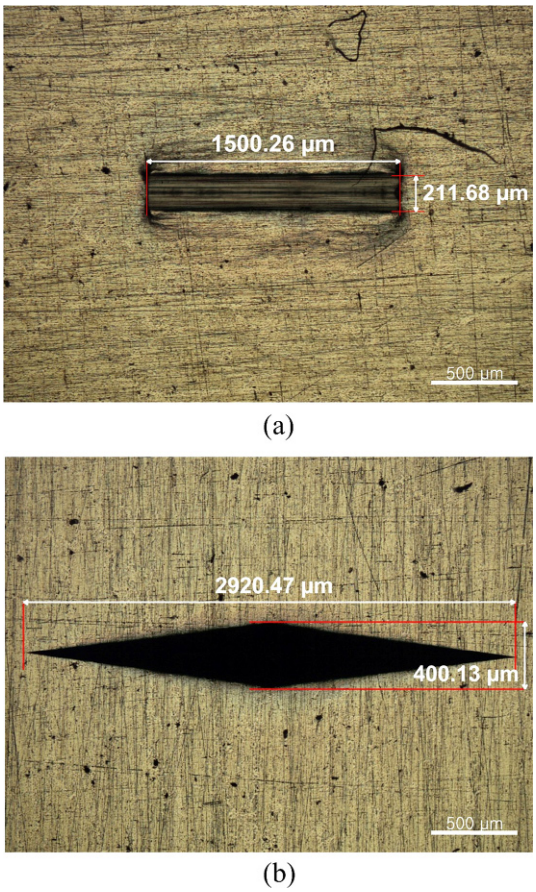

Fig. 6. Indent area optical images (× 50) of (a) wedge indenter and (b) Knoop indenter after indentation test with 100 μm indentation depth.

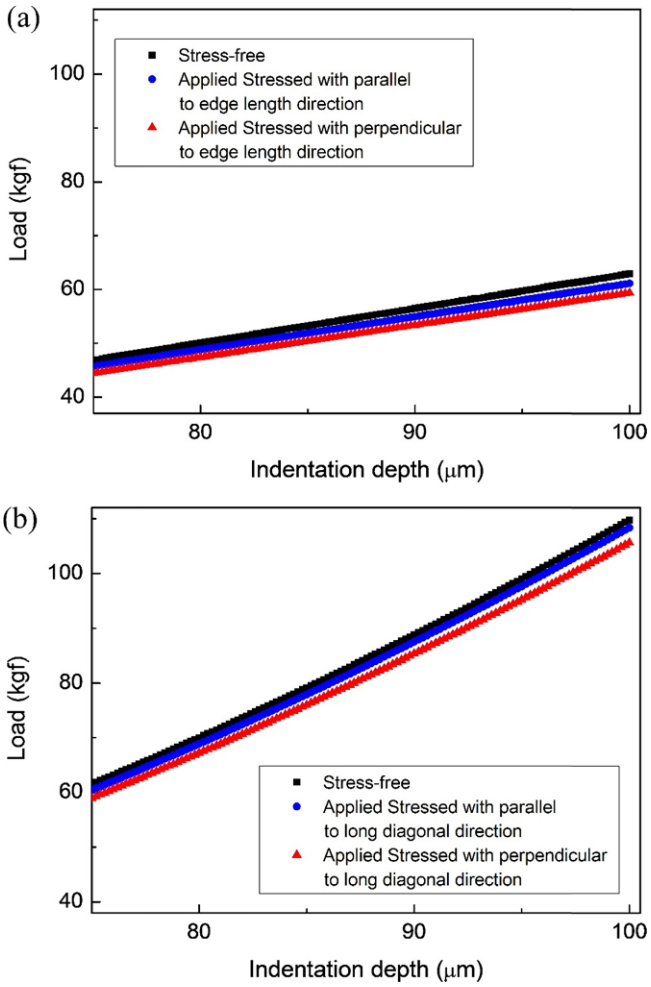

Fig. 7. Indentation load-depth curve on stress free specimen (black) and 180 MPa uniaxial tensile residual stressed specimen (two directions: red, blue) with (a) wedge indenter and (b) Knoop indenter.

depth are 2920.47 μm and 400.13 μm. The indent length of edge length with wedge indenter is 51% that of the long diagonal with Knoop indenter, and the included angle length with the wedge indenter is 53% that of the short diagonal with Knoop indenter.

To consider the load difference sensitivity on residual stress to the exclusion of experimental errors, wedge indentation tests and Knoop indentations on two principal directions were simulated on a stress-free specimen and a specimen in a 180 MPa uniaxial tensile stress state. The results show that the load differences of wedge indenter at 100 μm indentation depth are 3.54 kgf, and 1.79 kgf, and those for Knoop indenter are 4.14 kgf and 1.42 kgf (Fig. 8). Although the indenter lengths and indent impressions are both mostly reduced by half, we get the similar load difference values, showing that this approach for increasing residual stress sensitivity is reasonable. Since in many industrial situation like curved pipe or welding regions in the field, it is difficult to obtain enough flat indent area for two time Knoop indentation testing, the wedge indentation model is of interest in evaluating the residual stress directionality in-field. In addition, because of edge length and included angle van be chosen, and because of the simple shape of indenter, micro- and nanoscale extensions for thin films are expected.

The linear relationship among ΔL_x, ΔL_y and applied stress (75 MPa, 150 MPa, 203 MPa, and 270 MPa, $p = 0$) was proportionally determined by experiment. Figure 9 shows the load differences (ΔL_x, ΔL_y) between the stress-free and applied stress states. The simulation were supplemented with linear relationship between two load differences and applied stress (150 MPa, 180 MPa and 250 MPa, $p = 0$). The S45C specimen with 150 MPa applied stress was intended to match the experimental data, and the purpose of considering material STS 303 was to examine the feasibility of developed model extending our model to another types of materials. The size of specimen was 8 mm in the included angle direction (x-direction), 8 mm in the edge length direction (z-direction), and 4 mm in the indenting direction (y-direction). The mesh of the specimen beneath indenter was made up of a mesh region size 0.031 mm in the x-direction, 0.031 mm in the z-direction and 0.016 mm in the y-direction. The entire zone size with fine mesh was 0.50 mm, 3.0 mm, and 0.25 mm in the x-, z-, and y- directions, respec-

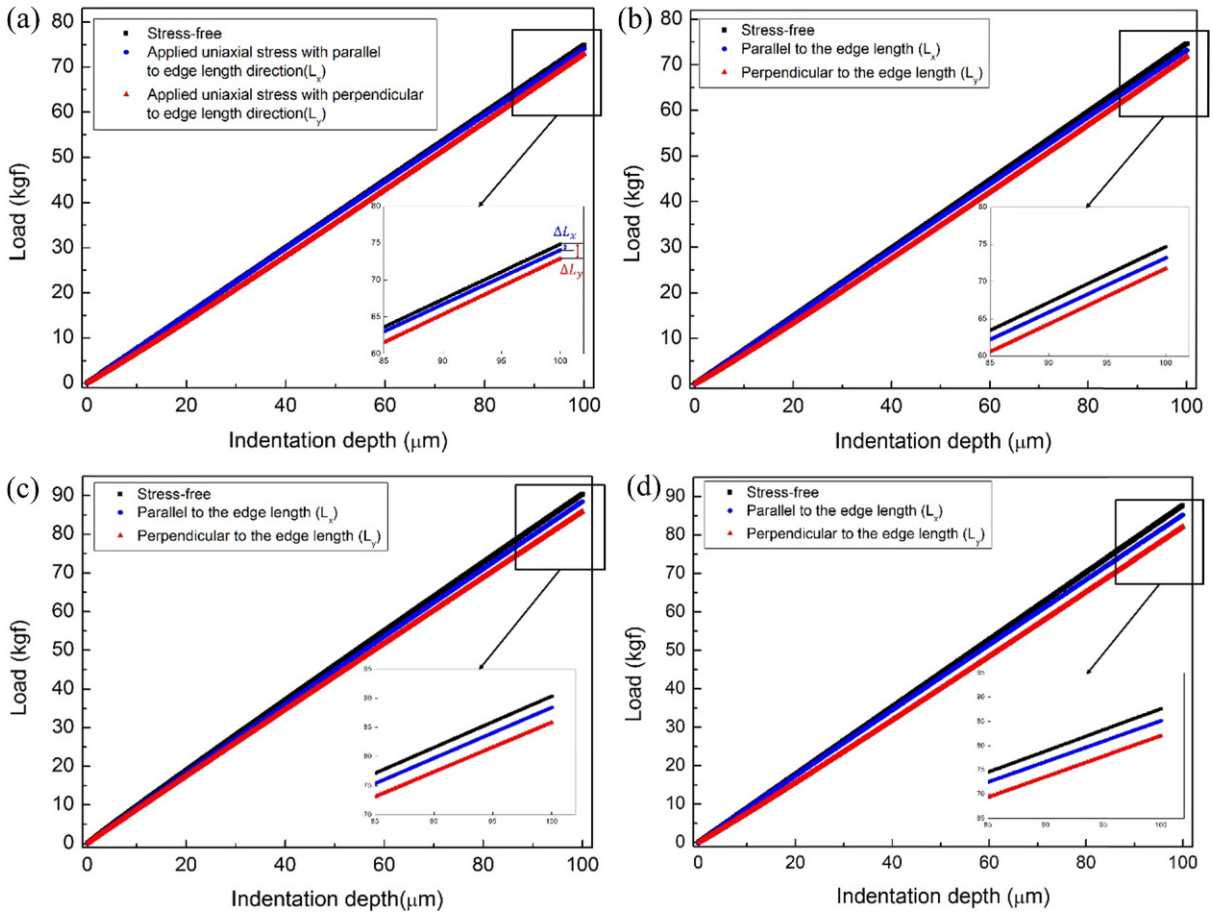

Fig. 8. Indentation load-depth curves of stress-free (black) and stressed specimen (two directions: red, blue). (a) S45C with 75 MPa uniaxial tensile stress, (b) S45C with 150 MPa uniaxial tensile stress, (c) SKD11 with 203 MPa uniaxial tensile stress, and (d) SCM4 with 270 MPa uniaxial tensile stress.

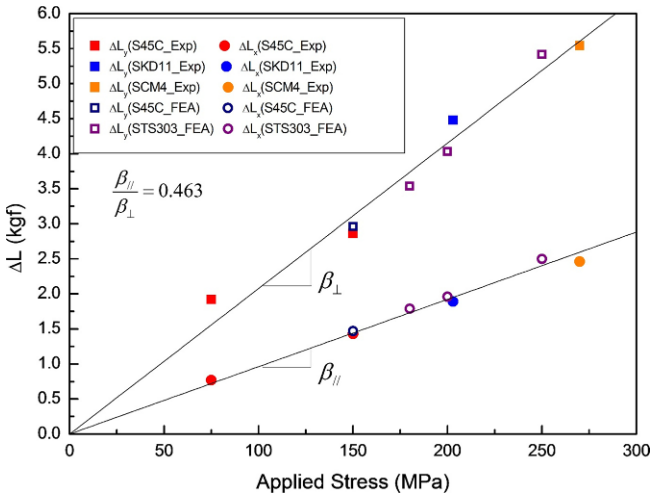

Fig. 9. Relationship between applied stresses and load differences.

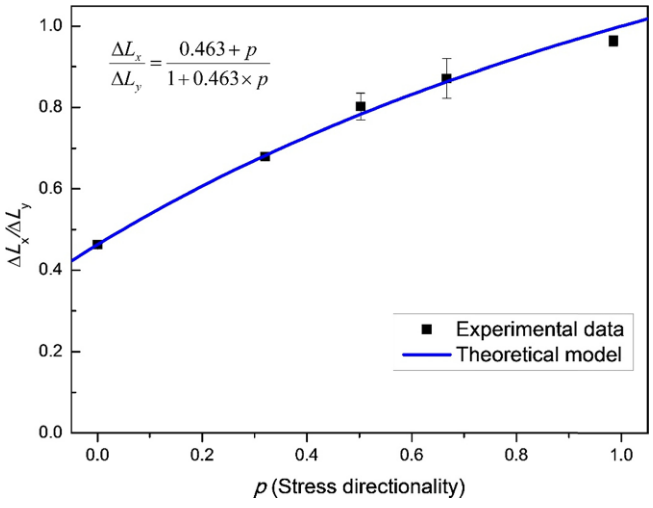

Fig. 10. Verification of wedge indentation model with various stress directionalities.

tively, and as in Fig. 6(b), it covers the region directly penetrated by the indenter, and the highly deformed region that occurs in sink-in or pile up in indentation testing. For effective analysis, the mesh size increases with distance from the indenter.

The linear relation from experiments and simulations is shown in Fig. 10, where the slope of the graph is the conversion factor

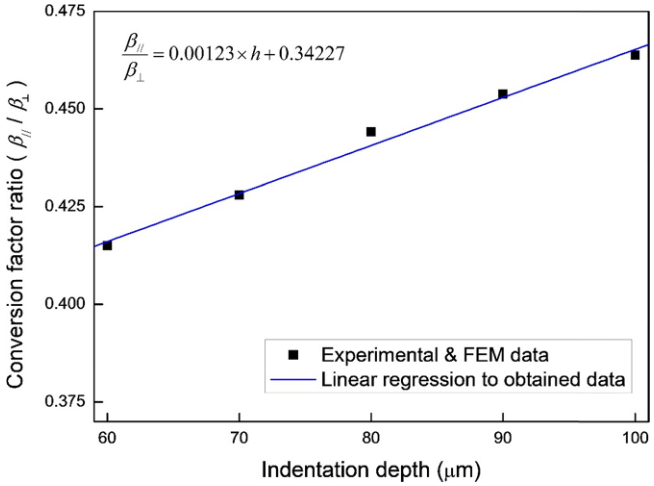

Fig. 11. Linear relationship between indentation depth and conversion factor ratio.

on each direction. The conversion factor ratio, $\beta_{//}/\beta_{\perp}$, was 0.463 at 100 μm indentation depth regardless of applied stress. The verification of the wedge indentation model, specimens with uniaxial, equibiaxial and nonequibiaxial residual stresses were performed according to the experimental condition of Table 2. In all tensile applied stress states, the experimental results were in agreement with the theoretical model (Eq. (6)) with conversion factor ratio 0.463 (Fig. 11). From the experimental results for various materials and biaxial stress states, we can deduce that the conversion factor of wedge indenter does not depend on the material or biaxial stress state.

Let us consider the relationship between depth and conversion factor ratio. In case of the Knoop indenter [12], the conversion factor ratio ($\alpha_{//}/\alpha_{\perp}$) converges to 0.34 independent of indentation depth because of the indenter's geometrical self-similarity. However, as the wedge indenter does not have geometrical self-similarity, it shows a linear relationship between the conversion factor ratio and indentation depth (Fig. 12). Previous research [16] suggests that the conversion factor is related to the plastic zone area perpendicular to the residual stress. However, the absence of analyzing on plastic zone size beneath wedge indenter, the discussion on the relationship between conversion factor ratio and indentation depth is qualitatively analyzed. We suppose that the conversion factor ratio is related to the subjected indenter areas which is normal to the residual stress. There are two shapes in a wedge indenter: triangular in include angle direction and rectangular in edge length direction, respectively. The area of the triangular direction is proportional to the square of the indentation depth. On the other hand, the area of the rectangular side is proportional only to indentation depth. Since the conversion factor ratio is related to the two areas, we consider the linear relationship between conversion factor ratio and indentation depth a reasonable result.

The work presented here does not consider various included angles, and edge lengths, and further work on angle and length effects will be needed for wide application of wedge indentation testing.

5. CONCLUSION

In order to quantify stress directionality p with small indent area, the novel indentation model was verified with a wedge indenter. Instrumented wedge indentation testing in about one fourth indent area comparing to previous research, the linear relationship between uniaxial residual stress state and the load difference was confirmed, and we could obtain the conversion factors from the slopes in the plotted graph. Several experiments and FEM simulations on various uniaxial stress states showed that the conversion factor ratio had a constant value at 100 μm indentation depth regardless of material and applied stress. Instrumented wedge indentation tests on several uniaxial, equibiaxial, and nonequibiaxial residual stress state were performed, and the experimental results were verified by comparison with the theoretical modeling. In order to promote availability of the wedge indenter, a change of conversion factor ratio on indentation depth was considered. Unlike instrumented Knoop indentation testing, the conversion factor ratio of wedge indenter had a depth-dependency expressed by a linear fitting equation on indentation depth. This research will reduce the limitation on indent size in residual stress evaluation with instrumented indentation testing and it expand the in-field applicability of instrumented indentation testing.

ACKNOWLEDGEMENT

This work was supported by the Energy Efficiency & Resources Core Technology Program of the Korea Institute of Energy Technology Evaluation and Planning (KETEP) granted financial resource from the Ministry of Trade, Industry & Energy, Republic of Korea (No. 20141510101640). This work was supported by the National Research Foundation of Korea (NRF) grant funded by the Ministry of Science, ICT & Future Planning (MSIP) (NO. NRF-2015R1A5A1037627).

REFERENCES

1. I. C. Noyan and J. B. Cohen, *Residual Stress*, pp.13-46, Springer-Verlag, New York, USA (1987).
2. G. Totten, M. Howes, and T. Inoue, *Handbook of Residual Stress and Deformation of Steel*, pp.27-53, ASM International, Ohio, USA (1996).
3. Y.-H .Lee, S. Ahn, J.-Y. Kim, C.-P. Park, and H.-K. Jang, *Korean J. Met. Mater.* **53**, 162 (2015).
4. Y.-H. Lee, J. S. Park, Y. Kim, and Y.-H. Huh, *Korean J. Met. Mater*. **53**, 90 (2015).

5. T. Y. Tsui, W. C. Oliver, and G. M. Pharr, *J. Mater. Res*. **11**, 752 (1996).
6. A. Bolshakov, W. C. Oliver, and G. M. Pharr, *J. Mater. Res*. **11**, 760 (1996).
7. S. Suresh and A. E. Giannakopoulos, *Acta Mater*. **46**, 5755 (1998).
8. J. G. Swadener, B. Taljat, and G. M. Pharr, *J. Mater. Res*. **16**, 2091 (2001).
9. A. E. Giannakopoulos, *J. Appl. Mech*. **70**, 638 (2003).
10. Y.-H. Lee and D. Kwon, *Scripta Mater*. **49**, 459 (2003).
11. J.-I. Jang, *J. Ceram. Process. Res*. **10**, 291 (2009).
12. Y.-H. Lee and D. Kwon, *Acta Mater*. **52**, 1555 (2004).
13. Y.-H. Lee, K. Takashima, Y. Higo, and D. Kwon, *Scripta Mater*. **49**, 459 (2003).
14. J.-H. Han, J.-S. Lee, Y.-H. Lee, M.-J. Choi, G. Lee, D. Kwon, *et al. Key Eng. Mat.* **345-346**, 1125 (2007).
15. M.-J. Choi, S.-K. Kang, I. Kang, and D. Kwon, *J. Mater. Res*. **27**, 1 (2011).
16. Y.-C. Kim, M.-J. Choi, D. Kwon, and J.-Y. Kim, *Met. Mater. Int.* **21**, 850 (2015).
17. Y.-C. Kim, H.-J. Ahn, D. Kwon, and J.-Y. Kim, *Met. Mater. Int.* **22**, 12 (2016).